Asian Journal of Agriculture and Biology
https://doi.org/10.35495/ajab.2025.305

Original Article

In silico analyses of zingibain fibrinolytic mechanisms of ginger (*Zingiber officinale*)

Jonathan Suciono Purnomo[1], Richelle Clarence Saptura[1], Dikson[1], Dela Rosa[2], Ariela Samantha[1], Reinhard Pinontoan[1]*

[1]Department of Biology, Faculty of Health Science, Universitas Pelita Harapan, Jl. Jendral Sudirman 20, Lippo Karawaci, Tangerang 15810, Banten, Indonesia

[2]Department of Pharmacy, Faculty of Health Science, Universitas Pelita Harapan. Jl. Jendral Sudirman 20, Lippo Karawaci, Tangerang 15810, Banten, Indonesia

**Corresponding author's email:* reinhard.pinontoan@uph.edu

Received: 15 November 2025 / Revised: 25 March 2026 / Accepted: 30 March 2026 / Published Online: 09 April 2026

Abstract

Thrombosis is a major cause of cardiovascular diseases, contributing significantly to global mortality rates. It has become necessary to develop more cost-effective and safer treatments for thrombosis, such as those derived from plants, due to prohibitively high costs and severe side effects of existing medications. Ginger (*Zingiber officinale*) has been reported to have thrombolytic abilities via fibrinolysis *in vitro*. Subsequently, the *in silico* studies described herein aimed to further understand the fibrinolytic mechanisms of zingibain-2 at the molecular level through molecular docking and dynamics simulations. AlphaFold3 accurately predicted the zingibain-2 structure and stably predicted the fibrin peptide-zingibain interactions. A preference for proline at the P2 position, typical of cysteine proteases, was found in 18, 8-residue peptides screened from human fibrin chains (PDB: 2HLO). Protein superimposition between the AlphaFold3 prediction and X-ray crystallography structures showed a minimum root mean square deviation value of 0.33 Å and 97.72% favorable residue orientation on a Ramachandran plot. Initial docking identified 13 out of 18, 8-residue human fibrin peptides with short catalytic distances. However, GROMACS molecular dynamics simulations of these AlphaFold3-docked complexes over 100 ns further narrowed this down to 11 out of 18, 8-residue human fibrin peptides with stable interactions, as demonstrated by their reliably short catalytic distances and negative binding energy. These stable models showed close, stable interactions with zingibain-2, and thus, support its potential as a plant-based thrombolytic agent. However, this must be experimentally validated.

Keywords: Fibrinolytic mechanism, Molecular docking, Molecular dynamics, Thrombolytic, Zingibain

How to cite this article:

Purnomo JS, Saptura RC, Dikson, Rosa D, Samantha A and Pinontoan R. *In silico* analyses of zingibain fibrinolytic mechanisms of ginger (*Zingiber officinale*). Asian J. Agric. Biol. 2026: e2025305. DOI: https://doi.org/10.35495/ajab.2025.305

Introduction

In 2021, approximately 18.9 million deaths or 31% of global deaths were attributed to cardiovascular disease (CVD) (World Health Organization, 2025). A significant proportion of these CVDs are associated with thrombosis, which involves the formation of blood clots that obstruct blood vessels and impair tissue oxygenation. If left untreated, thrombosis can result in severe complications, such as stroke, coronary artery disease, deep vein thrombosis, and pulmonary embolism (World Health Organization, 2025; Ashorobi et al., 2024). There are at least three known classes of thrombolytic medications used for rapidly treating thrombosis: antiplatelets, which slow down platelet and thrombin activities; anticoagulants, which enhance endogenous thrombolytic processes; and fibrinolytics, which degrade fibrin fibers that hold the thrombi together (Mackman et al., 2020). However, these treatments are often prohibitively costly and are associated with allergic reactions and other side effects, prompting the search for safer, more affordable alternatives derived from natural sources (Baig and Bodle, 2023).

Plant-derived proteolytic enzymes have attracted attention as potential thrombolytic agents becasue of their ability to degrade fibrin. Various studies have been carried out to demonstrate the fibrinolytic activities of plant-based cysteine proteases, which include *Actinidia deliciosa* actinidin, *Carica papaya* papain, and *Ananas comosus* bromelain (Pinontoan et al., 2024; Purnomo et al., 2025; Ramli et al., 2018). Ginger (*Zingiber officinale*) has long been used in traditional medicine to support circulatory health. Its rhizomes contain two cysteine protease isoforms known as zingibain-1 and zingibain-2, which exhibit strong protein hydrolyzing activity. Previous studies have reported that crude extracts of ginger rhizomes possess fibrinolytic activity *in vitro* (Pinontoan et al., 2024).

Despite these findings, the molecular mechanisms underlying the interaction between zingibain-2 and fibrin substrates is yet to be better understood. Its catalytic mechanisms are extrapolated from its sibling cysteine protease enzymes, such as actinidin, papain, and bromelain. Their conserved histidine-cysteine-asparagine triads or histidine-cysteine dyads have been reported to play important roles in proteolytic activity. Histidine deprotonates cysteine to allow nucleophilic attack on the scissile bond. In certain cysteine protease clans, however, the asparagine residue may be necessary to orient and stabilize the histidine's imidazolium ring for successful catalysis (Ramli et al., 2018; Choi et al., 1999; Choi and Laursen, 2000; Oanca et al., 2020; Pinontoan et al., 2024; Purnomo et al., 2025). Understanding how zingibain-2 recognizes and interacts with fibrin peptides is essential for elucidating its fibrinolytic mechanism at the molecular level. Fibrin, derived from fibrinogen during blood clot formation, contains peptide segments that serve as targets for proteolytic enzymes. Proteases typically recognize their substrates through amino acid residues surrounding the cleavage site, commonly described using the Schechter and Berger nomenclature (P4–P1 / P1′–P4′). Investigating fibrin-derived peptide segments, therefore, provides a useful framework for understanding the substrate recognition mechanism of zingibain-2. Recent advances in computational biology have enabled the investigation of enzyme–substrate interactions at atomic resolution through in silico approaches. Techniques such as molecular docking and molecular dynamics (MD) simulations allow the exploration of catalytic interactions, structural stability, and binding behavior of enzyme–substrate complexes under simulated physiological conditions. These computational methods have become powerful tools for studying enzyme mechanisms and predicting protein–substrate interactions prior to experimental validation (Śledź and Caflisch, 2018; Markovic et al., 2020).

In silico analysis offers an important step in addressing the underlying zingibain-2–fibrin interaction at the molecular level, to better understand its fibrinolytic mechanism of action. *In silico* experiments harness computational power, computer software, and publicly available biological databases. A recent example is the selection, retrieval, and comprehensive *in silico* analyses of *Bacillus* fibrinolytic enzyme sequences and respective studies of their structures, amino acid compositions, and physicochemical properties, with the aim of attaining a better picture of the sequence–property relationships of *Bacillus* fibrinolytic enzymes and the creation of mutant enzymes better-suited for specific applications (Boro et al., 2024). Within the context of this study, *in silico* experiments simulate molecular behavior and interactions between biological macromolecules, *i.e.,* enzyme-peptide catalytic reactions, within a specified space and specified chemical and physical conditions and time. These *in silico* experiments involve molecular docking and MD simulations to provide insights for initial *in*

https://doi.org/10.35495/ajab.2025.305

vitro experiments and to validate prior *in vitro* experiments. Conversely, *in silico* experiments can and should be validated with subsequent *in vitro* experiments. By combining the strengths of both approaches, *in silico* experiments can validate and focus *in vitro* experiments, and therefore, reduce laboratory resource and time usage (Purnomo et al., 2025). As such, this study aimed to elucidate the molecular interactions between *Z. officinale* zingibain-2 and fibrin-derived peptides through *in silico* molecular docking and MD simulation approaches already established in prior studies of actinidin and papain enzymes and to evaluate the effectiveness of *Z. officinale* zingibain-2 as a potential plant-based thrombolytic agent.

Material and Methods

Fibrin peptide scissile bond prediction

Scissile bonds within fibrin were predicted based on the human fibrin structure available in the Protein Data Bank (PDB ID: 2HLO) (Doolittle et al., 2006), which represents a fragment of the fibrin D-dimer relevant to physiological clot formation. Chains A (α), B (β), and C (γ) of one asymmetric unit were analyzed, with residue numbering following the PDB 2HLO coordinate numbering system (Doolittle et al., 2006). Only residues with resolved atomic coordinates were included, while regions lacking electron density or peptide ligands were excluded to ensure structural consistency for downstream simulations. Potential cleavage sites were identified by scanning for peptide segments in which proline was present at the P2 position, in accordance with the substrate specificity of zingibain-2, which cleaves the peptide bond between P1 and P1′ residues (Choi et al., 1999). Residue positions around the scissile bond were annotated following the nomenclature described by Schechter and Berger, in which substrate residues interacting with protease subsites may extend beyond the immediate scissile bond (P1–P1′) and include positions up to P4–P4′ (Schechter and Berger, 1967; Waldner et al., 2018). Each candidate scissile bond was extended to include residues P4–P4′, resulting in octameric peptide segments (P4–P3–P2–P1–P1′–P2′–P3′–P4′), which were used as substrates in subsequent molecular docking and MD simulations with zingibain-2.

AlphaFold3 prediction of zingibain structure

Zingibain isoform 2 (zingibain-2) was selected because of the availability of its crystallographic structure (PDB ID: 1CQD), which enabled direct structural validation because of its 100% sequence identity with the experimental template (Choi et al., 1999). The amino acid sequence (UniProt accession P82474) comprises 221 residues, corresponding exactly to the crystallographic structure determined by X-ray diffraction at 2.10 Å resolution, with reported R-work and R-free values of 0.213 and 0.249, respectively. Three-dimensional structure prediction was performed using the AlphaFold3 server, with the full-length 221-residue sequence as the input, under default parameters (Abramson et al., 2024). Prior to complex modeling with fibrin peptides, the reliability of the predicted structure was evaluated by superimposition onto the crystallographic reference structure (PDB ID: 1CQD) using PyMOL v3.1.6.1 (Schrödinger and DeLano, 2020). Structural similarity between the predicted and experimental models was quantified by calculating the root mean square deviation (RMSD) of the backbone atoms following structural alignment. Stereochemical quality was assessed using Ramachandran plot analysis generated via the SWISS-MODEL server (Sobolev et al., 2020). Additional structural validation was performed using ERRAT (Colovos and Yeates, 1993) and VERIFY3D (Bowie et al., 1991; Lüthy et al., 1992) through the SAVES v6.0 server to evaluate the overall reliability of the AlphaFold3 model against the experimentally resolved model.

Zingibain-fibrin peptide molecular docking simulation

Molecular docking interactions between zingibain-2 and the 8-residue fibrin peptides (P4–P4′) were modeled using the AlphaFold3 server (Abramson et al., 2024). The full-length amino acid sequences of zingibain-2 (UniProt P82474) and each peptide were submitted to the AlphaFold3 server under default parameters to generate enzyme–peptide complex structures. AlphaFold3 predicts protein–protein interactions using a neural network architecture capable of modeling inter- and intra-molecular residue relationships and refining atomic coordinates through a diffusion-based structural prediction framework (Abramson et al., 2024). For each enzyme–peptide pair, five structural models were generated (Abramson et al., 2024). Structural visualization and analysis were

performed using PyMOL (Schrödinger and DeLano, 2020). The catalytic triad of zingibain-2 (Cys27, His161, and Asn181) was defined based on the crystallographic structure (PDB ID: 1CQD) (Choi et al., 1999). This catalytic arrangement corresponds to the conserved Cys–His–Asn catalytic motif characteristic of papain-like cysteine proteases belonging to the C1 family (clan CA), according to the MEROPS peptidase database (Rawlings et al., 2017), whereas the histidine residue activates the catalytic cysteine nucleophile and the asparagine residue stabilizes the histidine during catalysis (Ramli et al., 2018). For each enzyme-peptide pair, five models were generated. The representative docking model for each complex was selected based on catalytic feasibility. Specifically, the distance between the sulfur atom (SG) of Cys27 and the carbonyl carbon of the P1 residue of the peptide was measured. The model exhibiting the shortest distance was selected as the most plausible cleavage orientation. AlphaFold3 docking confidence metrics, including the predicted template modeling (pTM), interface pTM (ipTM) scores, combined confidence score, and predicted local distance difference test (pLDDT) value were also evaluated. The pLDDT values were extracted directly from the AlphaFold3 output. The combined confidence score however, was calculated from the pTM and ipTM scores, weighted to favor the latter, as described by Evans et al. (2022) and Jumper et al. (2021) using Equation (1):

$$\mathbf{Confidence} = (\mathbf{0.8} \times \mathbf{ipTM}) + (\mathbf{0.2} \times \mathbf{pTM}) \quad \textbf{(1)}$$

The solvent-accessible surface area (SASA) of the peptide within each enzyme–peptide complex was calculated using PyMOL to estimate substrate exposure within the catalytic pocket. The selected complexes were subsequently subjected to MD simulations to allow structural relaxation and conformational refinement prior to trajectory analysis through further MD simulations.

MD simulation

MD simulations were performed using GROMACS version 2023.4 with the CHARMM36-jul2022 force field (Abraham et al., 2015), with parameters adapted from our previous study, to analyze the interactions between zingibain-2 and the docked fibrin peptides (Pinontoan et al., 2024). The system selected for the simulation comprised the best docking model as determined based on the SG–C distance in the zingibain-2–fibrin peptide complex solvated in a cubic water box using the SPC/E water model (Berendsen et al., 1987). To ensure system stability, a minimum distance of approximately 3.0 nm was maintained between any protein atom and the box boundary. The simulation began with energy minimization to stabilize the initial configuration, NVT equilibration (constant volume and temperature) at 298 K for 100 ps, and NPT equilibration (constant particle count, pressure, and temperature) for 300 ps. The temperature gradually increased to 310 K. The bond lengths were constrained using the LINCS algorithm, and long-range electrostatic interactions used the particle mesh Ewald method with a 160 pm grid (Essmann et al., 1995; Hess et al., 1998). The production simulation was conducted for 100 ns with a 2-fs timestep. Throughout the simulation, the RMSD and Z-score normalized root mean square fluctuation ($RMSF_N$) of the enzyme and peptide were monitored and calculated to evaluate conformational changes (Essmann et al., 1995). Additionally, the distance between Cys27-SG of zingibain-2 and P1-C of the fibrin peptide was tracked to observe the catalytic interaction.

The binding affinities of the zingibain-2–fibrin peptide complexes were calculated as the Gibbs binding free energy (ΔG) in kcal/mol using gmx_mmpbsa software (Valdés-Tresanco et al., 2021) with the molecular mechanics/generalized born surface area (MM/GBSA) method, as used in prior *in silico* MD analyses of papain enzymes (Valdés-Tresanco et al., 2021; Purnomo et al., 2025). The equations for this calculation are expressed as Equations (2) and (3):

$$\mathbf{\Delta G^{o}_{MM/GBSA}} = \mathbf{[G_{complex}]} - \mathbf{[G_{enzyme}]} - \mathbf{[G_{peptide}]} \quad \textbf{(2)}$$

with

$$\mathbf{G_x} = \mathbf{[E_{MM}]} + \mathbf{[G_{solvation}]} - \mathbf{[TS]} \quad \textbf{(3)}$$

The MM/GBSA Gibbs binding free energy is a delta between an enzyme–peptide complex system and the sum of the enzyme and peptide systems, represented by G_x terms, with each term being the sum of the molecular mechanical energy of the system represented by E_{MM} and the solvation energy represented by $G_{solvation}$, from which the product of the system's temperature and entropy, represented by T and S, respectively, is subtracted. Binding free energy

calculations were performed using snapshots extracted from the last 20 ns of the simulation at 100 ps intervals.

Results

Fibrin peptide scissile bond prediction

Potential cleavage sites targeted by zingibain-2 were identified based on its reported preference for proline residues at the P2 position (Choi et al., 1999). Using a fragment of the human fibrin D-dimer crystal structure (PDB ID: 2HLO) as a reference, fibrin chains were screened for residues satisfying these motifs. Eighteen potential scissile bonds were identified across the fibrin chains. Of these, 10 peptide segments originated from the fibrin Bβ chain, while eight were derived from the fibrin Cγ chain (Table 1). No candidate peptides were detected in the fibrin Aα chain because of the absence of proline residues at the P2 position. Eighteen potential scissile bonds were identified and subsequently expanded into 8-residue peptide sequences encompassing the P4–P4′ positions. Of these, 10 peptides originated from the fibrin Bβ chain and eight from the fibrin Cγ chain, as summarized in Table 1. No scissile bonds were identified in the fibrin Aα chain, because no proline residues were present at the P2 position. Therefore, no 8-residue peptides from the Aα chain were generated for further analysis. Each candidate cleavage site was extended to include residues spanning the P4–P4′ positions, resulting in 8-residue peptide segments used for subsequent molecular docking and MD simulations.

Table-1. Predicted cleavable 8-residue peptide sequences.

Fibrin chain	Fibrin peptide	Peptide sequences	Predicted cleavage sites (P1–P1′)
FibAα	FibAα	-	-
FibBβ	FibBβ-1	NIPTNLRV	Thr163–Asn164
	FibBβ-2	RTPCTVSC	Cys197–Thr198
	FibBβ-3	NIPVVSGK	Val205–Val206
	FibBβ-4	IQPDSSVK	Asp230–Ser231
	FibBβ-5	VKPYRVYC	Tyr236–Arg237
	FibBβ-6	WDPYKQGF	Tyr269–Lys270
	FibBβ-7	GLPGEYWL	Gly290–Glu291
	FibBβ-8	MGPTELLI	Thr308–Glu309
	FibBβ-9	SDPRKQCS	Arg391–Lys392
	FibBβ-10	ANPNGRYY	Asn413–Gly414
FibCγ	FibCγ-1	QEPCKDTV	Cys139–Lys140
	FibCγ-2	IKPLKANQ	Leu172–Lys173
	FibCγ-3	LSPTGTTE	Thr221–Gly222
	FibCγ-4	AIPYALRV	Tyr244–Ala245
	FibCγ-5	VGPEADKY	Glu270–Ala271
	FibCγ-6	DDPSDKFF	Ser300–Asp301
	FibCγ-7	STPNGYDN	Asn361–Gly362
	FibCγ-8	IIPFNRLT	Phe389–Asn390

Structural validation of the zingibain-2 model

The three-dimensional structure of zingibain-2 (PDB: 1CQD) was predicted using AlphaFold3 (Choi et al., 1999; Abramson et al., 2024). The structure was evaluated for its suitability for subsequent docking simulations using two approaches: 1) structural superimposition with the experimentally resolved X-ray crystallography structure to calculate the RMSD, which assesses the overall similarity and ensures the predicted model does not deviate significantly from the native conformation, and 2) Ramachandran plot analysis to evaluate the stereochemical quality and backbone conformations of the protein residues (Sobolev et al., 2020; Pan et al., 2025). In the Ramachandran plots (Figure 1B, C), each dot represents an individual residue, and the contour lines (first, second, and third) indicate favored and allowed backbone conformations based on confidence levels,

namely, the most favored regions (99.7%), additionally allowed regions (95.0%), and generously allowed regions (80.0%) (Ramachandran et al., 1963). Structural superimposition of the predicted model with the experimentally resolved X-ray crystallography structure showed a low RMSD value of 0.33 Å (Figure 1A). Furthermore, the AlphaFold3-predicted structure showed favorable conformations, as indicated by the Ramachandran plot showing 97.72% of residues with favorable torsional angles, without any outliers (Figure 1B), which was in agreement with the experimentally resolved structure shown in the Ramachandran plot in Figure 1C. Further validation using ERRAT resulted in an overall quality factor of 98.58%, which exceeded the commonly accepted threshold for high-resolution structures (> 95%). VERIFY3D analysis demonstrated that 81.90% of residues achieved a 3D–1D score ≥ 0.1, surpassing the 80% acceptance criterion for structural compatibility. These results demonstrated high structural agreement between the predicted and experimentally resolved structures, supporting the reliability of the AlphaFold3 model for subsequent molecular docking and MD simulations (Terefe and Ghosh, 2022).

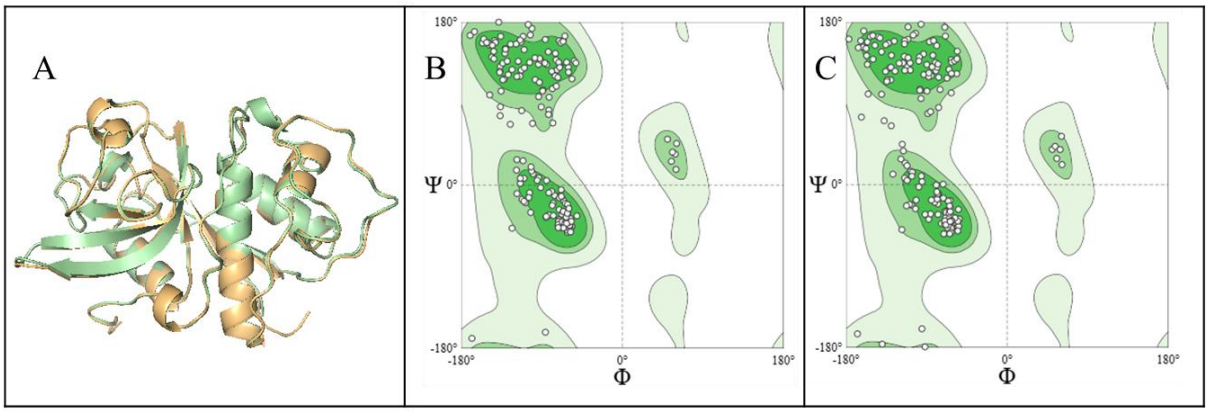

Figure-1. Structural validation of the AlphaFold3-predicted zingibain-2 model. (A) Structural superimposition of the predicted model (green) with the experimentally resolved X-ray crystal structure (PDB: 1CQD, orange). (B) Ramachandran plot of the predicted structure. (C) Ramachandran plot of the crystallographic reference structure.

AlphaFold3-predicted docking of zingibain–2 with fibrin peptides

Docking simulations were performed by predicting complexes between zingibain-2 and each of the 18 candidate fibrin peptides using AlphaFold3. The selected docking poses are shown in Figure 2. In all complexes, the fibrin peptides were positioned within the catalytic cleft of zingibain-2, near the catalytic triad residues Cys27, His161, and Asn181. The orientation of the peptide backbone relative to the catalytic residues suggested plausible geometries for nucleophilic attack at the P1–P1′ peptide bond (Choi and Laursen, 2000). The protein–peptide complex models were further validated using the benchmarking metrics of AlphaFold3, as predicted pTM and ipTM scores, as outlined by Jumper et al. (2021). Both metrics were combined into ipTM-weighted confidence values (Evans et al., 2022).

Table 2 shows the AlphaFold3-predicted protein–peptide docking interactions between zingibain-2 and 8-residue human fibrin peptides benchmarked for their accuracy based on pLDDT, pTM, ipTM, and ipTM-weighted confidence scores. The predicted complexes exhibited high pLDDT values (91.62–94.92), indicating reliable local structural accuracy of the modeled residues (Guo et al., 2022). The overall fold confidence, as reflected by the pTM values, remained consistently high across all complexes (0.93–0.95), supporting the structural integrity of the predicted enzyme–peptide models. The interface confidence (ipTM) scores ranged from 0.45 to 0.86. Although ipTM values above 0.8 are generally associated with highly reliable protein–protein interfaces, lower scores are frequently observed in protein–peptide systems because of the smaller interaction surface area (Varga et al., 2025). To further rank the docking models, an ipTM-weighted confidence score was calculated, yielding values between 0.56 and 0.93. For initial catalytic assessment, the distance between Cys27 SG and the P1 carbonyl atoms was measured, with distances ≤ 5 Å considered permissive for potential

cleavage. All complexes were subsequently subjected to MD simulations to allow structural relaxation and refinement, enabling even moderate-confidence models to adopt catalytically favorable geometries.

Table-2. AlphaFold3 confidence scores of the predicted zingibain-2–peptide complexes.

Fibrin peptide	pLDDT	ipTM	pTM	Confidence
FibAα	-	-	-	-
FibBβ-1	93.18	0.53	0.94	0.63
FibBβ-2	94.27	0.52	0.94	0.62
FibBβ-3	94.27	0.54	0.93	0.63
FibBβ-4	93.20	0.45	0.93	0.56
FibBβ-5	94.75	0.79	0.94	0.84
FibBβ-6	92.73	0.63	0.94	0.71
FibBβ-7	92.55	0.69	0.94	0.76
FibBβ-8	94.92	0.90	0.95	0.93
FibBβ-9	93.77	0.56	0.94	0.65
FibBβ-10	93.23	0.61	0.94	0.69
Fibγ-1	93.46	0.56	0.94	0.65
Fibγ-2	94.00	0.60	0.94	0.68
Fibγ-3	93.57	0.60	0.94	0.69
Fibγ-4	91.62	0.62	0.93	0.70
Fibγ-5	93.43	0.63	0.94	0.71
Fibγ-6	91.92	0.53	0.93	0.63
Fibγ-7	93.59	0.50	0.94	0.61
Fibγ-8	93.36	0.52	0.94	0.62

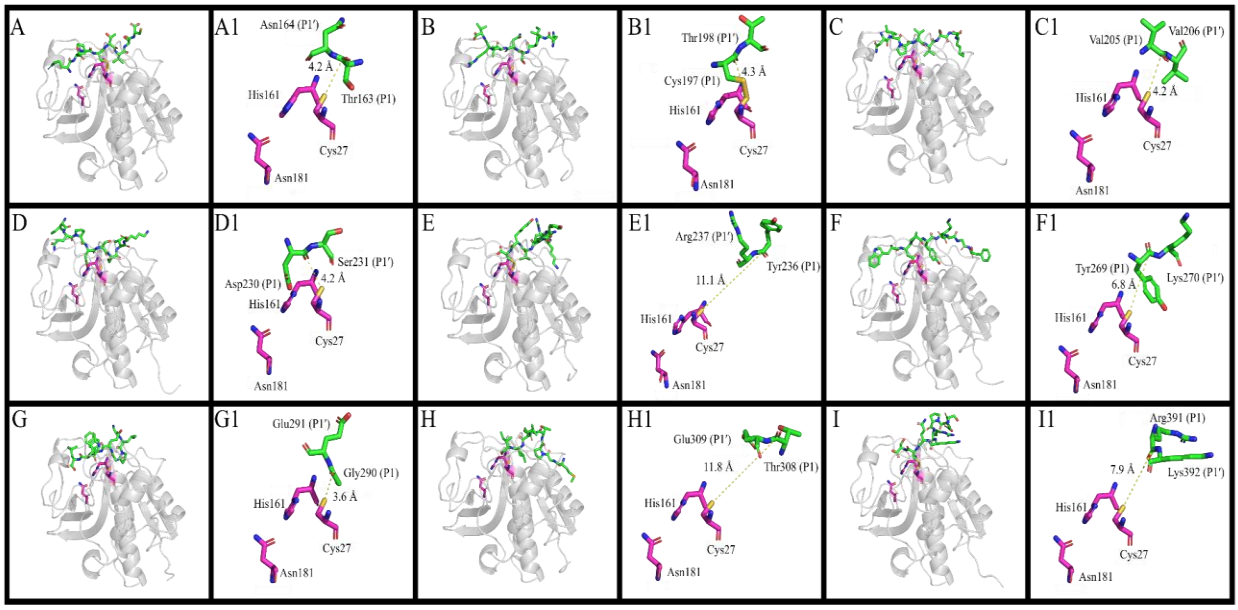

https://doi.org/10.35495/ajab.2025.305

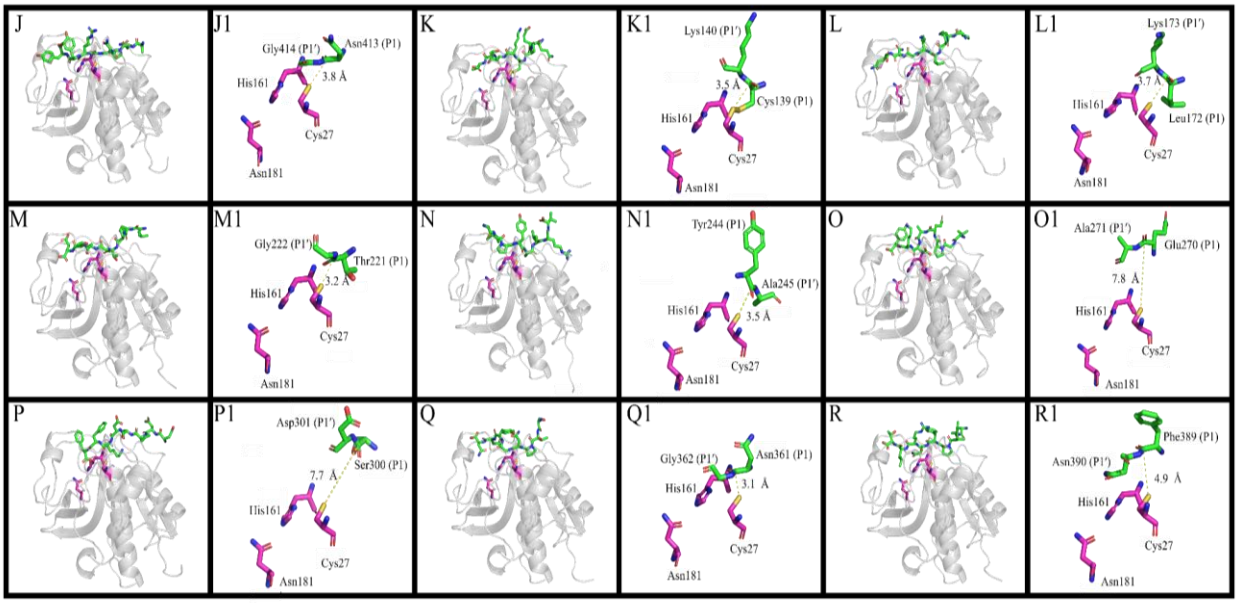

Figure-2. Molecular docking results between zingibain-2 (gray) and fibrin β-chain peptides (green). The catalytic triad residues of zingibain-2 (Cys27, His161, and Asn181) are highlighted in magenta. Yellow dashed lines indicate the distance (Å) between the sulfur atom (SG) of Cys27 and the carbon atom (C) of the P1 residue at the target peptide bond. (A–J) Binding conformations of fibrin β peptides (FibBβ-1 to FibBβ-10). (A1–J1) Corresponding zoomed interaction views showing key residues and interaction distances. (K–R) Binding conformations of fibrin γ peptides (FibCγ-1 to FibCγ-8). (K1–R1) Corresponding zoomed interaction views showing key residues and interaction distances.

To determine whether the predicted complexes adopted catalytically favorable orientations, the distance between the sulfur atom (SG) of Cys27 and the carbonyl carbon (C) of the peptide P1 residue was measured. The catalytic distances between the Cys27-SG and P1-C atoms of zingibain-2 ranged from 3.1 to 11.8 Å (Figure 2). The closest onpeptideses were Fibγ-7 (3.1 Å) and Fibγ-3 (3.2 Å), followed by Fibγ-4, Fibγ-1, and Fibγ-5 at approximately 3.5 Å; FibBβ-7 (3.6 Å); Fibγ-2 (3.7 Å); and FibBβ-10 (3.8 Å). Peptides FibBβ-1, FibBβ-4, FibBβ-3, FibBβ-2, and Fibγ-8 were further away (4.2–4.9 Å), and the furthest peptides were FibBβ-6, Fibγ-6, FibBβ-9, FibBβ-5, and FibBβ-8 (6.8–11.8 Å). Thirteen of the peptides were also found to be within the reported ≤ 5 Å threshold for catalytic competence, with six from the Bβ chain and seven from the γ chain, and thus, they were considered catalytically favored for cleavage (Pinontoan et al., 2024). The zingibain-2-peptide interaction SASA was measured to evaluate the peptides' accessibility within the zingibain-2 catalytic pocket (Table 3). FibBβ-5 exhibited the highest SASA value (941.203 Å²), while Fibγ-3 showed the lowest SASA value (716.703 Å²). Thus, these peptides, respectively, have better and worse solvent accessibility (Mukherjee and Bahadur, 2018). The remaining peptides displayed intermediate SASA values within this range, reflecting varying degrees of exposure of the scissile bond to the enzyme (Venkatraman et al., 2009).

Table-3. Predicted SASA values of the fibrin peptides.

Fibrin peptide	SASA (Å²)
FibAα	-
FibBβ-1	855.640
FibBβ-2	750.853
FibBβ-3	751.487
FibBβ-4	770.653
FibBβ-5	941.203
FibBβ-6	763.416
FibBβ-8	816.430
FibBβ-9	813.699
FibBβ-10	758.144
FibCγ-1	818.466
FibCγ-2	847.795
FibCγ-3	716.703
FibCγ-4	829.281
FibCγ-5	778.401
FibCγ-6	834.777
FibCγ-7	755.874
FibCγ-8	909.921

MD stability of zingibain-2–peptide complexes

MD simulations were performed to evaluate the stability of zingibain-2–fibrin peptide interactions under dynamic conditions over time following the initial docking predictions. The MD simulation results were analyzed using several parameters, namely RMSD, $RMSF_N$, the catalytic distances between the active residues of zingibain-2 and fibrin peptides, and the binding free energy calculated using the MM/GBSA method.

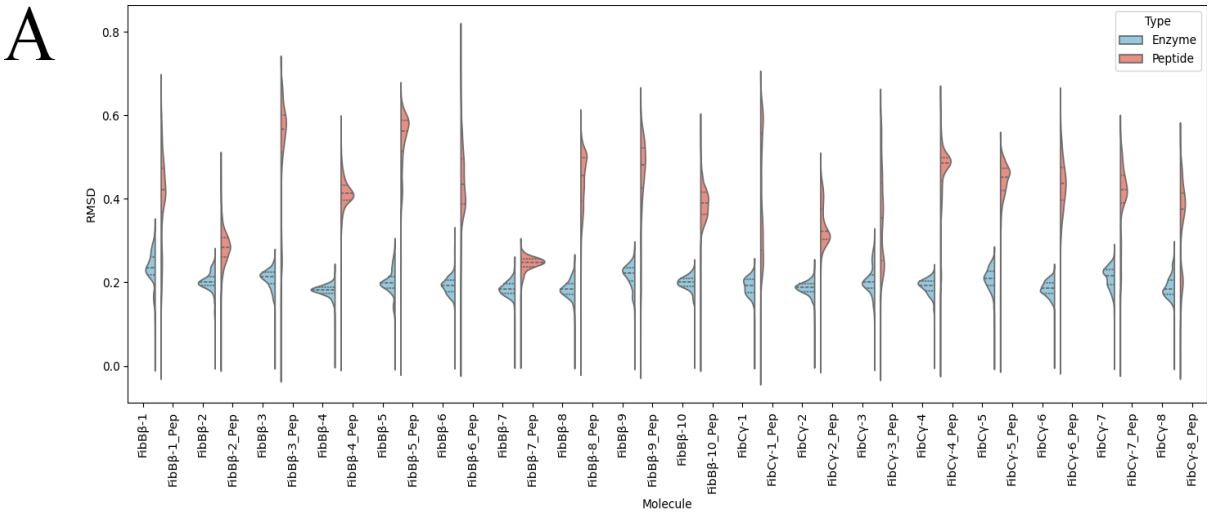

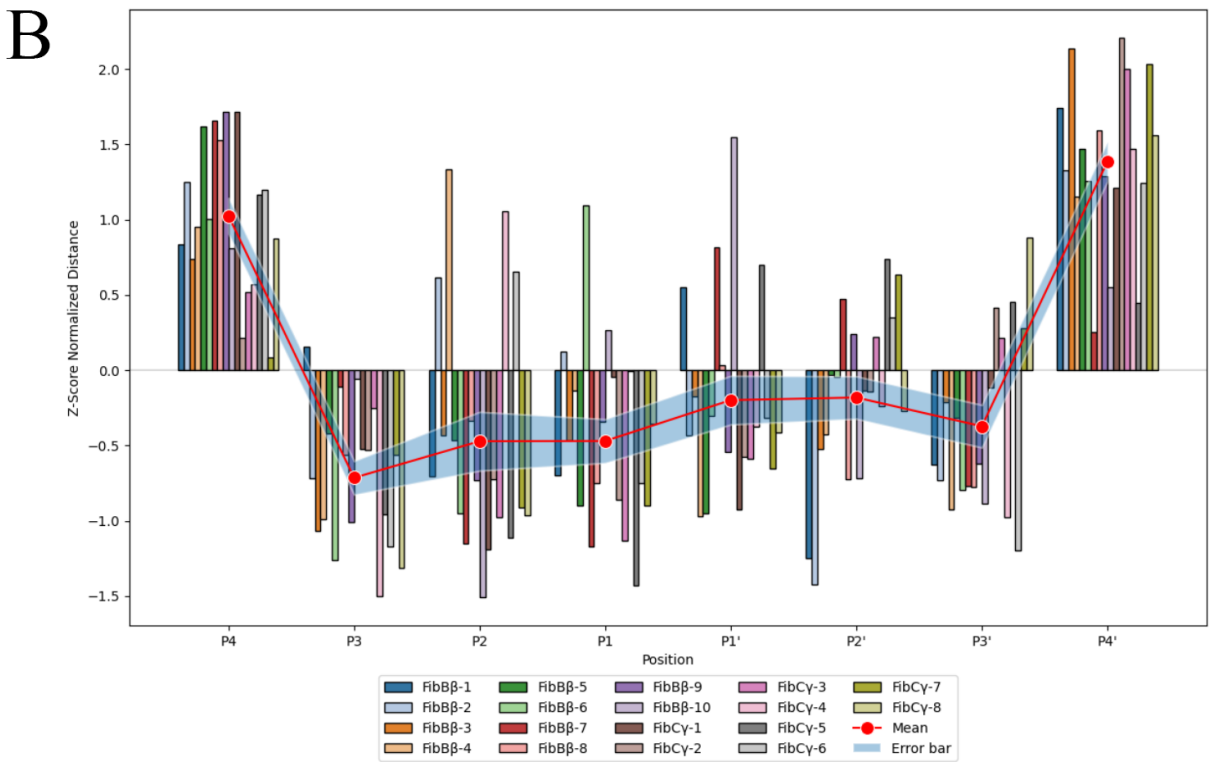

Figure-3. Molecular dynamics (MD) analysis of zingibain-2–peptide interactions. (A) Root mean square deviation (RMSD) violin plots showing the distribution of structural deviations of zingibain-2 (blue) and individual fibrin peptides (red) over a 100 ns simulation, where the x-axis represents each peptide–enzyme complex and the y-axis indicates the RMSD values (nm). (B) Normalized root mean square fluctuation ($RMSF_N$) of Cα atoms for each amino acid residue in the fibrin peptides according to substrate positions relative to the scissile bond (P4–P4′). The x-axis denotes residue positions within the peptide, whereas the y-axis represents normalized $RMSF_N$ values.

The structural behavior of zingibain-2 and the fibrin peptides was monitored throughout the 100-ns MD simulation and displayed as RMSD violin plots to assess their molecular stability, based on how far they deviated from their initial conformation. Lower values indicated a more rigid structure (Bhattacharya et al., 2024). While the zingibain-2 RMSD value reflects its overall structural integrity, the peptide RMSD reflects its own integrity within the zingibain-2 binding site throughout the simulation. As shown in Figure 3A, zingibain-2 (blue) consistently exhibited low RMSD values across all simulations, indicating that the enzyme structure remained stable throughout the simulation, indicating a stable catalytic geometry integrity. In contrast, the peptides (red) were found to be much more flexible, as reflected by higher and broader RMSD distributions. Despite this variability, most peptides exhibited RMSD values concentrated in a single dominant population, indicating that they remained associated with the enzyme throughout most of the simulation. Fibγ-1 and Fibγ-8 peptides however, demonstrated bimodal RMSD distributions, which likely suggested an intermittent loss of a stable binding pose, because of temporary displacement from the catalytic site.

$RMSF_N$ analysis of Cα atoms was performed for every amino acid in the fibrin peptides to evaluate residue-level flexibility. This analysis quantifies the deviations of atom positions from their average during MD simulations (Figure 3B). Increased flexibility is indicated by higher $RMSF_N$ values (Bagewadi et al., 2023; Song et al., 2024). The residue positions were numbered before and after the cleavage point, in accordance with the method described by Schechter and Berger (1967). In this nomenclature, the peptide bond targeted for cleavage is located between the P1 and P1′ positions, with numbers P4–P1 from the N-terminal side and P1'–P4' to the C-terminal side. The

https://doi.org/10.35495/ajab.2025.305

residues closest to the cleavage site (P3–P3′) are regarded as belonging to the central binding region, whereas P4 and P4′ represent the peptide's terminal ends. The terminal residues, P4 and P4', showed much higher $RMSF_N$ values, whereas the inner residues showed lower values. This indicates that the substrate-binding pocket preferentially recognizes the inner residues, forming multiple interactions that stabilize them. Such stabilization increases the likelihood that these residues adopt the correct orientation for proteolysis. Therefore, consistently low $RMSF_N$ values are indicative of the enzyme effectively recognizing and securing the peptide within the pocket, enabling proper orientation and enhancing the probability of cleavage. However, not all peptides follow this phenomenon. Certain peptides, including FibBβ-1, FibBβ-2, FibBβ-4, FibBβ-6, FibBβ-7, FibBβ-9, FibBβ-10, FibCγ-3, FibCγ-4, FibCγ-5, FibCγ-6, and FibCγ-7, had one or more of their inner residues exhibiting higher $RMSF_N$ values, suggesting potential flexibility that may affect the scissile bond orientation.

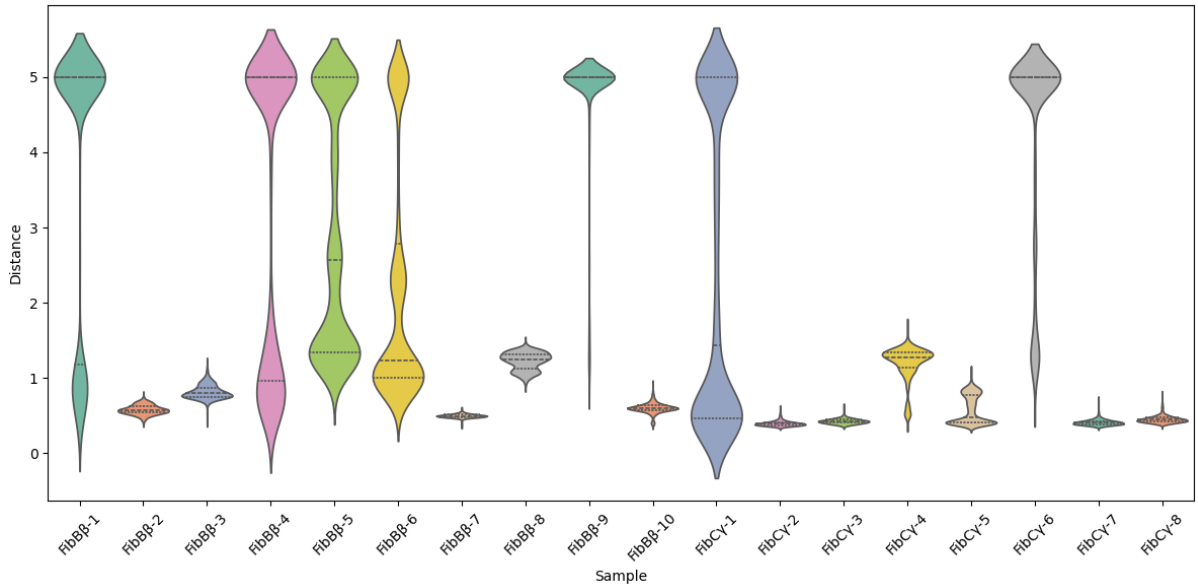

Figure-4. Violin plot of the catalytic distance between Cys27-SG of zingibain-2 and P1-C of the fibrin peptides over 100 ns of MD simulations.

Catalytic distance analysis was performed to evaluate whether the catalytic interaction between zingibain-2 and the fibrin peptides could be maintained consistently under dynamic conditions during the MD simulation. The distribution of the catalytic distance between the SG atom of the catalytic Cys27 residue of zingibain-2 and the carbonyl carbon at the P1 position of each fibrin peptide over the 100-ns simulation was visualized using violin plots (Figure 4). Eleven of the 18 peptides maintained a catalytic distance less than ~2 Å, maintaining stable interactions within the catalytic pocket, which suggests a favorable orientation for nucleophilic attack and thus, a higher likelihood of being cleavable substrates (Cuesta et al., 2020; Ochoa et al., 2020). In contrast, seven peptides displayed broader distributions and/or frequent sampling distances greater than 4 Å. These peptides, including Fibβ-1, Fibβ-4, Fibβ-5, Fibβ-6, and Fibγ-1, showed wider bimodal distributions and larger interquartile ranges, which suggested their temporary binding within the catalytic site before dissociation occurred at some point throughout the simulation trajectory. Peptides Fibβ-9 and Fibγ-6 were even outright dissociated from the enzyme shortly after the simulation started, becasue of their much narrower distribution and a median at 5 Å.

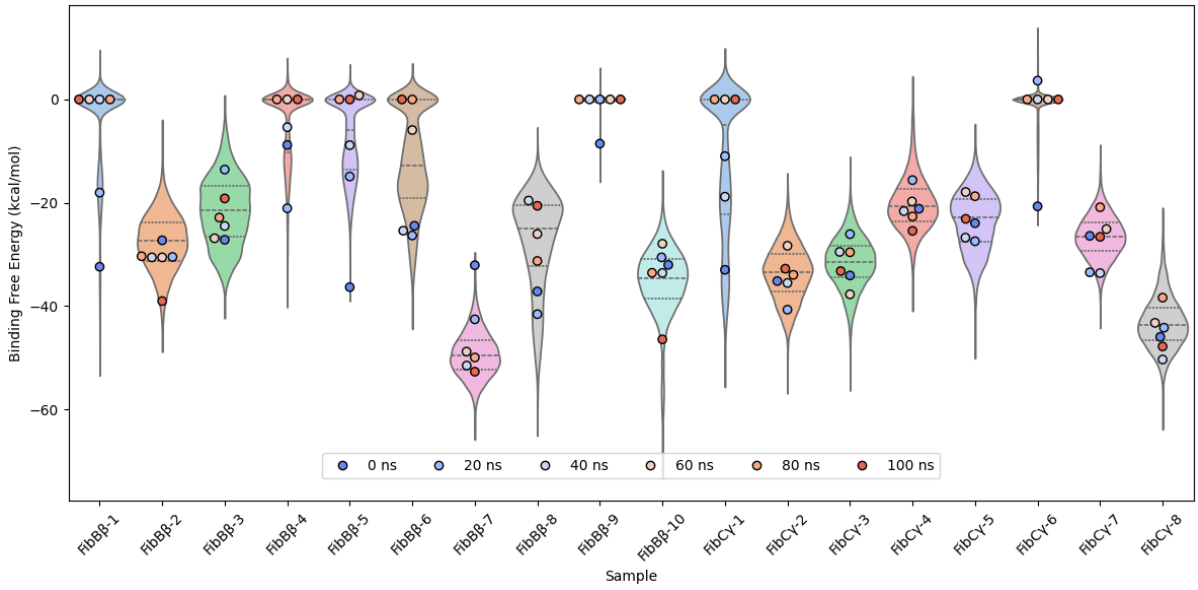

Figure-5. Violin plot of molecular mechanics/generalized born surface area binding free energy analysis from MD simulations of 18 zingibain-2–peptide interactions. Colored dots represent binding free energy values sampled at 20 ns intervals throughout the simulation.

In addition to the RMSD, RMSF, and catalytic distance, the MM/GBSA free binding energies of these zingibain-2–peptide interactions were estimated by combining molecular mechanics energies with solvation terms (Kollman et al., 2000). Energetically favorable interactions, indicated by negative binding free energy values, are much more favored for stable and successful catalytic reactions. In contrast, near-zero or positive energy values indicate much weaker binding and therefore, may risk dissociation (Bello et al., 2025). As shown in Figure 5, 11 of the 18 peptides indicated favorable interactions through their consistently negative energies throughout the MD simulation, while the remainder indicated much weaker interactions, or even dissociation, given that their energies fluctuated towards zero.

Discussion

In silico analyses provide valuable insights into enzyme–substrate recognition mechanisms that are often difficult to capture experimentally. In the present study, a combination of AlphaFold3-based docking and MD simulations was used to investigate how zingibain-2 interacts with fibrin-derived peptides at the molecular level. These analyses extend previous *in vitro* observations of fibrinolytic activity performed by Pinontoan et al. (2024) by providing structural and dynamic evidence supporting the catalytic capability of zingibain-2 toward fibrin substrates. Before analyzing enzyme–substrate interactions, the structural reliability of the predicted zingibain-2 model was evaluated. The AlphaFold3-predicted zingibain-2 structure displayed excellent structural similarities with the crystallographic reference model (PDB: 1CQD), as indicated by the low RMSD value, favorable Ramachandran-plotted torsional angles, and high ERRAT and VERIFY3D benchmarking scores (Pan et al., 2025; Sobolev et al., 2020; Colovos and Yeates, 1993; Bowie et al., 1991; Lüthy et al., 1992). These findings confirmed that the predicted structure accurately reproduces the experimentally resolved fold of zingibain-2 and therefore, provides a reliable framework for analyzing substrate-binding interactions. Moreover, the findings are in line with earlier studies showing the robustness of AlphaFold-based protein predictions (Jumper et al., 2021).

Following structural validation, docking simulations revealed that 13 of the 18 peptides could adopt binding orientations that place the scissile bond at a distance compatible with the catalytic triad of zingibain-2 (Cys27–His161–Asn181). In cysteine proteases such as zingibain-2, actinidin, bromelain and papain, His161 activates the thiol group of Cys27, enabling nucleophilic attack on the peptide bond, while Asn181 orients and stabilizes the imidazolium ring of the

catalytic histidine during the catalytic reaction (Choi et al., 1999; Oanca et al., 2020; Purnomo et al., 2025; Ramli et al., 2018). The observed positioning of fibrin peptides near this catalytic triad suggested that zingibain-2 can accommodate multiple fibrin-derived substrates within its active site. The veracity of these AlphaFold3-predicted enzyme–peptide complexes were further benchmarked using AlphaFold's internal metrics, including pLDDT, pTM, and ipTM scores. The models exhibited consistently high pLDDT values (> 91), indicating reliable local structural accuracy across both enzyme and peptide regions (Guo et al., 2022). This was supported by high pTM scores (0.93 to 0.95), indicating high global structural model reliability. iPTM values ranged from 0.45 to 0.90, which, although lower than those typically observed in protein–protein complexes, are consistent with the smaller interaction surface area of protein–peptide complexes (Evans et al., 2022; Jumper et al., 2021).

Substrate accessibility also appears to contribute to cleavage potential. The scissile bond must be sufficiently exposed on the peptide surface to permit enzymatic access, in addition to having a catalytic distance compatible with cleavage (Venkatraman et al., 2009). Thus, SASA measurements were performed on these 8-residue peptides to ascertain whether their cleavage sites were solvent-accessible or buried (Mukherjee and Bahadur, 2018). The peptides that showed both wide SASA values and short catalytic distances were Fibγ-4, Fibγ-1, and FibBβ-7. This implies that the scissile bonds are both close to Cys27 and sufficiently exposed to be catalyzed by the enzyme. The other peptides, however, displayed less ideal configurations by either staying highly exposed, but further away from Cys27, or being correctly oriented, but buried further within the active site.

Although molecular docking provides initial binding poses, it represents enzyme–substrate interactions only at a single time point and, therefore, does not reflect the inherent flexibility of proteins (Śledź and Caflisch, 2018). MD simulations, therefore, play a critical role in assessing whether these complexes remain catalytically competent under dynamic conditions, because proteases frequently experience conformational changes during catalysis (Hollingsworth and Dror, 2018). The low RMSD values observed during the simulation indicated that zingibain-2 maintained structural stability throughout the simulations. While the peptides themselves displayed more varied RMSD profiles, the complexes achieved catalytically stable states. These profiles indicated conformational adaptation within the catalytic pocket (Bello et al., 2025). Furthermore, these dynamic modifications were supported by the temporal fluctuations observed in the catalytic distance and binding free energy. Residue-level RMSF analysis revealed that residues located near the central cleavage region (P3–P3′) tended to display lower fluctuations compared to those observed for the terminal residues (P4 and P4′). This pattern suggested that the catalytic pocket stabilizes residues surrounding the scissile bond, while allowing greater flexibility at peptide termini, a behavior consistent with previously reported substrate recognition patterns in papain-like proteases. Liu et al. (2009) suggested that stabilization may help to maintain a peptide orientation favorable for the nucleophilic attack of Cys27. However, the peptides' end residues remained flexible. This suggested induced-fit adaptations that allow the enzyme to accept a range of peptide sequences without changing the catalytic geometry (Yang et al., 2017).

Throughout the course of 100 ns MD simulations, 11 out of the 18 peptides consistently maintained short catalytic distances and favorably negative binding free energies, suggesting geometries compatible with catalytic interactions. The remaining seven peptides, however, displayed less-stable interactions, with near-zero binding free energies and pronounced distance fluctuations that may have ended with sheer dissociation. Most of these peptides showed high $RMSF_N$ values at the central residues (P3–P3'), indicating that their flexibility might reduce their ability to bind to the enzyme. These results suggested that increased flexibility near the cleavage region may reduce the stability of enzyme–peptide interactions. Therefore, their decreased flexibility may be correlated with more stable enzyme–peptide interactions (Yang et al., 2017). More importantly, the distinct stability observed in peptides that satisfy the P2 proline requirement suggested that additional residues surrounding the scissile bond may facilitate more effective binding and, consequently, catalysis (Choe et al., 2006). This suggested that zingibain-2 substrate recognition likely involves contributions from flanking positions by adjacent residues, in addition to the canonical P2 proline motif, likely related to zingibain-2 positioning in cysteine protease clans.

The MD simulations suggested that zingibain-2 is capable of forming stable interactions with several fibrin-derived peptides in catalytically favorable

https://doi.org/10.35495/ajab.2025.305

geometries. While 11 of the 18 peptides exhibited < 2 Å Cys27-SG to P1-C catalytic distances, the remainder exhibited distances > 4 Å. These distance ranges are respectable compared to other papain-like cysteine proteases that have been reported to be fibrinolytic, such as papain, which exhibits catalytic distances > 3.3 Å, and actinidin, which exhibits catalytic distances of 3.6 and 4.4 Å throughout their respective MD simulations (Pinontoan et al., 2024; Purnomo et al., 2025). Papain and zingibain-2 both allow greater flexibility at P4 and P4' positions, while stabilizing residues around P3–P3' (Purnomo et al., 2025). These comparisons suggest that zingibain-2 shares molecular interaction behaviors with other plant cysteine proteases previously reported to possess fibrinolytic activity.

Despite these computational findings indicating the fibrinolytic activity of zingibain-2 against certain parts of the fibrin chain, it must be considered that this *in silico* study relied purely on computational simulations of the molecular-scale interaction between the enzyme and the fibrin peptides and as such, is predictive in nature. As such, the findings must be validated via *in vitro* experimentation to confirm the enzymatic activity of zingibain-2 and its mechanisms of action with human fibrin as the substrate. Furthermore, the therapeutic development of zingibain-2 as a fibrinolytic agent must also take pharmacological considerations into account, which are normally explored through *in vitro* and *in vivo* experiments beyond the scope of this *in silico* study (Sliwoski et al., 2014). Zingibain-2 may exhibit off-target proteolytic activity against non-fibrin targets, leading to undesirable systemic effects (Huber et al., 2025). Excessive fibrinolytic activity may exacerbate the risk of bleeding which is a common complication associated with thrombolytic therapy (Stewart and Kline, 2020). Immunogenicity and stability in physiological conditions also remain to be evaluated (Hazare et al., 2024). Therefore, safety evaluations are essential before considering therapeutic development.

Conclusion

Overall, these *in silico* analyses highlighted human fibrin peptides as potential catalytic targets of zingibain-2. Throughout the 100-ns MD simulations, 11 of the 18 peptides maintained favorably negative binding energies and short catalytic distances, with the P3–P3' central residues mostly stabilized to facilitate the nucleophilic attack of Cys27. These *in silico* results support the hypothesis that zingibain-2 has potential as a natural thrombolytic enzyme by demonstrating substrate recognition beyond the P2 proline motif and showing similar behavior to other plant-based cysteine proteases with fibrinolytic activity. However, these findings must be validated via *in vitro* experiments.

Acknowledgement

The authors acknowledge the financial support from The Indonesian Ministry of Higher Education, Science and Technology, Directorate General for Research and Development (1063/LL3/DT.06.01/2025) and LLPM (021/LPPM-UPH/VI/2025).

Disclaimer: None.

Conflict of Interest: None.

Source of Funding: Ministry of Education, Culture, Research and Technology of the Republic of Indonesia and LPPM UPH.

Use of Generative AI Tools Statement

We hereby declare that AI tools were utilized during the manuscript preparation process only for the purposes of: (i) checking spelling and grammatical structure using PaperPal and Grammarly, (ii) verifying the consistency and format of reference citations The authors maintained full responsibility for all content, and every section of the manuscript was carefully reviewed and revised to match current academic publishing guidelines.

Contribution of Authors

Purnomo JS & Pinontoan R: Conceptualized the study and designed research methodology.

Purnomo JS, Saptura RC & Dikson: Performed experiments, collected & analyzed data and manuscript write-up.

Samantha A, Rosa D & Pinontoan R: Reviewed and edited the manuscript and supervised the work.

All authors read and approved final draft of the manuscript.

References

Abraham MJ, Murtola T, Schulz R, Páll S, Smith JC, Hess B and Lindahl E, 2015. GROMACS: high performance molecular simulations through multi-level parallelism from laptops to

supercomputers. SoftwareX 1–2:19–25. DOI: https://doi.org/10.1016/j.softx.2015.06.001

Abramson J, Adler J, Dunger J, Evans R, Green T, Pritzel A, Ronneberger O, Willmore L, Ballard AJ, Bambrick J, Bodenstein SW, Evans DA, Hung CC, O'Neill M, Reiman D, Tunyasuvunakool K, Wu Z, Žemgulytė A, Arvaniti E, Beattie C, Bertolli O, Bridgland A, Cherepanov A, Congreve M, Cowen-Rivers AI, Cowie A, Figurnov M, Fuchs FB, Gladman H, Jain R, Khan YA, Low CMR, Perlin K, Potapenko A, Savy P, Singh S, Stecula A, Thillaisundaram A, Tong C, Yakneen S, Zhong ED, Zielinski M, Žídek A, Bapst V, Kohli P, Jaderberg M, Hassabis D and Jumper JM, 2024. Accurate structure prediction of biomolecular interactions with AlphaFold 3. Nature. 630:493–500. DOI: https://doi.org/10.1038/s41586-024-07487-w

Ashorobi D, Fernandez R and Ameer MA, 2024. Thrombosis [Internet]. PubMed. Treasure Island (FL): StatPearls Publishing; 2024 [cited 2025 Sep 28]. Available from: https://www.ncbi.nlm.nih.gov/books/NBK538430/

Bagewadi ZK, Yunus Khan TM, Gangadharappa B, Kamalapurkar A, Mohamed Shamsudeen S and Yaraguppi DA, 2023. Molecular dynamics and simulation analysis against superoxide dismutase (SOD) target of *Micrococcus luteus* with secondary metabolites from *Bacillus licheniformis* recognized by genome mining approach. Saudi J. Biol. Sci. 30(9):103753. DOI: https://doi.org/10.1016/j.sjbs.2023.103753

Baig MU and Bodle J, 2023. Thrombolytic Therapy [Internet]. National Library of Medicine. StatPearls Publishing; 2023 [cited 2025 Sep 28]. Available from: https://www.ncbi.nlm.nih.gov/books/NBK557411/

Bello AS, Uzairu A, Aadmu SG, Ibrahim A, Mahmood AA and Ibrahim MT, 2025. Molecular dynamics simulation, molecular docking, ADMET prediction, QSAR modeling and density functional theory computation for the identification of possible hepatitis C virus NS5B protease inhibitors through in silico study of fluorine-2, 7-diamine compounds. In Silico Res. Biomed. 1:100104. DOI: https://doi.org/10.1016/j.insi.2025.100104

Berendsen HJC, Grigera JR and Straatsma TP, 1987. The missing term in effective pair potentials. J. Phys. Chem. 91:6269–6271. DOI: https://doi.org/10.1021/j100308a038

Bhattacharya K, Chandra Nath B, Ahmed E, Khanal P, ChanuNR, Deka S, Das D and Shrivastava AK, 2024. Integration of network pharmacology, molecular docking, and simulations to evaluate phytochemicals from drymaria cordata against cervical cancer. RSC Adv. 14(6):4188–4200. DOI: https://doi.org/10.1039/d3ra06297j

Boro N, Fernandes PA and Mukherjee AK, 2024. Computational analysis to comprehend the structure-function properties of fibrinolytic enzymes from *Bacillus spp* for their efficient integration into industrial applications. Heliyon. 10(13): e33895. DOI: https://doi.org/10.1016/j.heliyon.2024.e33895

Bowie JU, Lüthy R and Eisenberg D, 1991. A method to identify protein sequences that fold into a known three-dimensional structure. Sci. 253(5016):164–170. DOI: https://doi.org/10.1126/science.1853201

Choe Y, Leonetti F, Greenbaum DC, Lecaille F, Bogyo M, Brömme D, Ellman JA and Craik CS, 2006. Substrate profiling of cysteine proteases using a combinatorial peptide library identifies functionally unique specificities. J. Biol. Chem. 281(18):12824–12832. DOI: https://doi.org/10.1074/jbc.m513331200

Choi KH, Laursen RA and Allen KN, 1999. The 2.1 Å structure of a cysteine protease with proline specificity from ginger rhizome, *Zingiber officinale*. Biochemistry. 38(36):11624–11633. DOI: https://doi.org/10.1021/bi990651b

Choi KH and Laursen RA, 2000. Amino-acid sequence and glycan structures of cysteine proteases with proline specificity from ginger rhizome *Zingiber officinale*. Eur. J. Biochem. 267:1516–1526. DOI: https://doi.org/10.1046/j.1432-1327.2000.01152.x

Colovos C and Yeates TO, 1993. Verification of protein structures: patterns of nonbonded atomic interactions. Protein Sci. 2(9):1511–1519. DOI: https://doi.org/10.1002/pro.5560020916

Cuesta S, Ferrater Mora J, Zambrano CH, Torres F and Rincón L, 2020. Comparative study of the nucleophilic attack step in the proteases catalytic activity: a theoretical study. Mol. Phys. 118 (14): e1705412. DOI: https://doi.org/10.1080/00268976.2019.1705412

Doolittle RF, Kollman JM, Chen A and Pandi L, 2006. Crystal structure of fragment D-dimer from human fibrin complexed with Gly-hydroxyPro-Arg-Pro-amide. Worldwide Protein Data Bank.

DOI: https://doi.org/10.2210/pdb2hlo/pdb

Essmann U, Perera L, Berkowitz ML, Darden T, Lee H and Pedersen LG, 1995. A smooth particle mesh Ewald method. J. Chem. Phys. 103:8577–8593. DOI: https://doi.org/10.1063/1.470117

Evans R, O'Neill M, Pritzel A, Antropova N, Senior A, Green T, Žídek A, Bates R, Blackwell S, Yim J, Ronneberger O, Bodenstein S, Zielinski M, Bridgland A, Potapenko A, Cowie A, Tunyasuvunakool K, Jain R, Clancy E, Kohli P, Jumper J and Hassabis D, 2022. Protein complex prediction with AlphaFold-Multimer. DeepMind. DOI: https://doi.org/10.1101/2021.10.04.463034

Guo H, Perminov A, Bekele S, Kedziora G, Farajollahi S, Varaljay V, Hinkle K, Molinero V, Meister K, Hung C, Dennis P, Kelley-Loughnane N and Berry R, 2022. AlphaFold2 models indicate that protein sequence determines both structure and dynamics. Sci. Rep. 12(1):10696. DOI: https://doi.org/10.1038/s41598-022-14382-9

Hazare C, Bhagwat P, Singh S and Pillai S, 2024. Diverse origins of fibrinolytic enzymes: A comprehensive review. Heliyon. 10(5): e26668. DOI: https://doi.org/10.1016/j.heliyon.2024.e26668

Hess B, Bekker H, Berendsen H and Fraaije, 1998. LINCS: A Linear Constraint Solver for molecular simulations. J. Comput. Chem. 18. DOI: 10.1002/ (SICI)1096-987X(199709)18:123.0.CO;2-H.

Hollingsworth SA and Dror RO, 2018. Molecular dynamics simulation for all. Neuron 99:1129–1143. DOI: https://doi.org/10.1016/j.neuron.2018.08.011

Huber L, Kucera T, Höllerer S, Borgwardt K, Panke S and Jeschek M, 2025. Data-driven protease engineering by DNA-recording and epistasis-aware machine learning. Nat. Commun. 16(1):5466. DOI: https://doi.org/10.1038/s41467-025-60622-7

Jumper J, Evans R, Pritzel A, Green T, Figurnov M, Ronneberger O, Tunyasuvunakool K, Bates R, Žídek A, Potapenko A, Bridgland A, Meyer C, Kohl SA, Ballard AJ, Cowie A, Romera-Paredes B, Nikolov S, Jain R, Adler J and Hassabis D, 2021. Highly accurate protein structure prediction with AlphaFold. Nature 596:583–589. DOI: https://doi.org/10.1038/s41586-021-03819-2

Kollman PA, Massova I, Reyes C, Kuhn B, Huo S, Chong L, Lee M, Lee T, Duan Y, Wang W, Donini O, Cieplak P, Srinivasan J, Case DA and Cheatham TE, 2000. Calculating structures and free energies of complex molecules: combining molecular mechanics and continuum models. Acc. Chem. Res. 33(12):889–897. DOI: https://doi.org/10.1021/ar000033j

Liu SQ, Meng ZH, Fu YX and Zhang KQ, 2009. Insights derived from molecular dynamics simulation into the molecular motions of serine protease proteinase K. J. Mol. Model. 16:17–28. DOI: https://doi.org/10.1007/s00894-009-0518-x

Lüthy R, Bowie JU and Eisenberg D, 1992. Assessment of protein models with three-dimensional profiles. Nature. 356(6364):83–85. DOI: https://doi.org/10.1038/356083a0

Mackman N, Bergmeier W, Stouffer GA and Weitz JI, 2020. Therapeutic strategies for thrombosis: new targets and approaches. Nat. Rev. Drug Discov. 19:333–352. DOI: https://doi.org/10.1038/s41573-020-0061-0

Markovic M, Ben-Shabat S and Dahan A, 2020. Computational simulations to guide enzyme-mediated prodrug activation. Int. J. Mol. Sci. 21(10):3621. DOI: https://doi.org/10.3390/ijms21103621

Mukherjee S and Bahadur RP, 2018. An account of solvent accessibility in protein-RNA recognition. Sci. Rep. 8:10546. DOI: https://doi.org/10.1038/s41598-018-28373-2

Oanca G, Asadi M, Saha A, Ramachandran B and Warshel A, 2020. Exploring the catalytic reaction of cysteine proteases. J. Phys. Chem. B. 124(50):11349–11356. DOI: https://doi.org/10.1021/acs.jpcb.0c08192

Ochoa R, Magnitov M, Laskowski RA, Cossio P and Thornton JM, 2020. An automated protocol for modelling peptide substrates to proteases. BMC Bioinform. 21(1):586. DOI: https://doi,org/10.1186/s12859-020-03931-6

Pan L, Wang A, Sang R, Lu X, Chen W, Ma Y and Deng F, 2025. AlphaFold 3 sheds insights into chemical enhancer-induced structural changes in CAS12A RNPS. Health Nanotechnol. 1(1). DOI: https://doi.org/10.1186/s44301-024-00003-z

Pinontoan R, Leke PAI, Lesmana JA, Purnomo JS, Dikson D and Samantha A, 2024. *In vitro* assessment of thrombolytic potential of red and white ginger (*Zingiber officinale*). Funct. Foods Health Dis. 14(1):62–73. DOI: https://doi.org/10.31989/ffhd.v14i1.1245

Pinontoan R, Purnomo JS, Avissa EB, Tanojo JP, Djuan M, Vidian V, Samantha A, Jo J and Steven E, 2024. In-vitro and in-silico analyses of the

thrombolytic potential of green kiwifruit. Sci. Rep. 14:13799. DOI: https://doi.org/10.1038/s41598-024-64160-y

Purnomo JS, Dikson, Soentoro SE, Erika, Sugata M, Samantha A and Pinontoan R, 2025. *In-silico* analysis of papain fibrinolytic mechanism from *Carica papaya*. Asia Pac. J. Mol. Biol. Biotechnol. 33(2):168–182. DOI: https://doi.org/10.35118/apjmbb.2025.033.2.17

Ramachandran GN, Ramakrishnan C and Sasisekharan V, 1963. Stereochemistry of polypeptide chain configurations. J. Mol. Biol. 7(1):95–99. DOI: https://doi.org/10.1016/s0022-2836(63)80023-6

Ramli ANM, Manas NHA, Hamid AAA, Hamid HA and Illias RM, 2018. Comparative structural analysis of fruit and stem bromelain from *Ananas comosus*. Food Chem. 266:183–191. DOI: https://doi.org/10.1016/j.foodchem.2018.05.125

Rawlings ND, Barrett AJ, Thomas, PD, Huang X, Bateman A and Finn RD, 2017. The MEROPS database of proteolytic enzymes, their substrates and inhibitors in 2017 and a comparison with peptidases in the PANTHER database. Nucleic Acids Res. 46(D1): D624–D632. DOI: https://doi.org/10.1093/nar/gkx1134

Schechter I and Berger A, 1967. On the size of the active site in proteases I Papain. Biochem. Biophys. Res. Commun. 27(2):157–162. DOI: https://doi.org/10.1016/s0006-291x(67)80055-x

Schrödinger L and DeLano W, 2020. PyMOL | www.pymol.org [Internet]. www.pymol.org. 2020 [cited 2025 Sep 29]. Available from: http://www.pymol.org/pymol

Śledź P and Caflisch A, 2018. Protein structure-based drug design: from docking to molecular dynamics. Curr. Opin. Struct. Biol. 48:93–102. DOI: https://doi.org/10.1016/j.sbi.2017.10.010

Sliwoski G, Kothiwale S, Meiler J and Lowe EW, 2014. Computational methods in drug discovery. Pharmacol. Rev. 66(1):334–395. DOI: https://doi.org/10.1124/pr.112.007336

Sobolev OV, Afonine PV, Moriarty NW, Hekkelman ML, Joosten RP, Perrakis A and Adams PD, 2020. A global Ramachandran score identifies protein structures with unlikely stereochemistry. Struct. 28:11–20. DOI: https://doi.org/10.1016/j.str.2020.08.005

Song X, Bao L, Feng C, Huang Q, Zhang F, Gao X and Han R, 2024. Accurate prediction of protein structural flexibility by deep learning integrating intricate atomic structures and Cryo-EM density information. Nat. Commun. 15:1–12. DOI: https://doi.org/10.1038/s41467-024-49858-x

Stewart LK and Kline JA, 2020. Fibrinolytics for the treatment of pulmonary embolism. Transl. Res. 225:82–94. DOI: https://doi.org/10.1016/j.trsl.2020.05.003

Terefe EM and Ghosh A, 2022. Molecular docking, validation, dynamics simulations, and pharmacokinetic prediction of phytochemicals isolated from *Croton dichogamus* against the HIV-1 reverse transcriptase. Bioinform. Biol. Insights 16. DOI: https://doi.org/10.1177/11779322221125605

Valdés-Tresanco MS, Valdés-Tresanco ME, Valiente PA and Moreno E, 2021. gmx_MMPBSA: A new tool to perform end-state free energy calculations with GROMACS. J. Chem. Theory Comput. 17(10):6281–6291. DOI: https://doi.org/10.1021/acs.jctc.1c00645

Varga JK, Ovchinnikov S and Schueler-Furman O, 2025. ActifpTM: a refined confidence metric of AlphaFold2 predictions involving flexible regions. Bioinformatics. 41(3): btaf107. DOI: https://doi.org/10.1093/bioinformatics/btaf107

Venkatraman P, Balakrishnan S, Rao S, Hooda Y and Pol S, 2009. A sequence and structure based method to predict putative substrates, functions and regulatory networks of endo proteases. PLoS ONE. 4(5): e5700. DOI: https://doi.org/10.1371/journal.pone.0005700

Waldner BJ, Kraml J, Kahler U, Spinn A, Schauperl M, Podewitz M, Fuchs JE, Cruciani G and Liedl KR, 2018. Electrostatic recognition in substrate binding to serine proteases. J Mol Recognit. 31(10): e2727. DOI: https://doi.org/10.1002/jmr.2727

World Health Organization, 2025. Cardiovascular diseases (CVDs) [Internet]. World Health Organization. 2025 [cited 2025 Sep 28]. Available from: https://www.who.int/news-room/fact-sheets/detail/cardiovascular-diseases-(cvds)

Yang LQ, Sang P, Zhang RP and Liu SQ, 2017. Substrate-induced changes in dynamics and molecular motions of cuticle-degrading serine protease PL646: a molecular dynamics study. RSC Adv. 7:42094–42104. DOI: https://doi.org/10.1039/c7ra07797a